

Axisymmetric Synthetic Jets: An Experimental and Theoretical Examination

Gopi Krishnan* and Kamran Mohseni†
University of Colorado, Boulder, Colorado 80309-0429

DOI: 10.2514/1.42967

The flowfield of a round synthetic jet driven by a piezoelectric membrane issuing into a quiescent environment is studied in this paper. The self-similar behavior exhibited by both synthetic and continuous turbulent jets leads to the hypothesis that synthetic jets may be modeled using similarity analysis, just as continuous turbulent jets are modeled. Accordingly, synthetic jets are modeled using both the Schlichting solution to boundary-layer equations in cylindrical coordinates and the Landau–Squire solution to the Navier–Stokes equations in spherical coordinates, for which the virtual viscosity coefficient of a continuous turbulent jet is replaced with that measured for a synthetic jet. The virtual viscosity of the synthetic jet for both models is obtained from the spreading rate and velocity decay rate of the jet. Hot-wire anemometry is used to characterize the flow downstream of the orifice. The flowfield is observed to consist of two regions, as distinguished by the centerline velocity decay: namely, a developing and a developed region. The developing region is characterized by a velocity increase followed by a plateau, for which the axial extent of this region scales with the stroke length L . The developed region is identified by the centerline velocity decaying as x^{-1} , and it is within this region that the jet models are applicable. The velocity decay rate and spreading rate of synthetic jets are observed to increase with stroke ratio L/d , while being independent of the Reynolds number Re . This dependency on stroke ratio is attributed to the increase in impulse and energy of the emerging vortex rings as the stroke ratio increases and their subsequent enhanced interaction. The geometry of the actuator is additionally seen to impact the spreading and decay rates by means of influencing the initial conditions at the orifice. The experiments verify that by using the adjusted value of the virtual viscosity, the theoretical models of a continuous turbulent jet may still be used to model a periodic synthetic jet. The virtual viscosity of the synthetic jets under test proves to be larger than that of equivalent turbulent continuous jet based on the same momentum flux. The enhanced viscosity is attributed to the additional momentum transfer and mixing brought about by the periodic introduction and breakdown of the vortex rings in synthetic jets.

Nomenclature

$b_{1/2}$	= half-width of the jet
D	= diameter of the cavity
d	= diameter of the orifice
F	= magnitude of the point force
f	= frequency of oscillation
H	= height of the cavity
h	= depth of the orifice
K	= kinematic momentum flux
K_b	= scaled jet spreading rate
K_u	= scaled velocity decay rate
L	= length of the slug
R	= radial coordinate (spherical polar coordinate)
Re	= Reynolds number
r	= radial coordinate (cylindrical polar coordinate)
S_b	= jet spreading rate
S_u	= velocity decay rate
T	= time period of oscillation
U_o	= mean actuator exit velocity
u	= mean streamwise velocity (cylindrical polar coordinate)
u_c	= mean streamwise centerline axial velocity
u_r	= mean radial velocity (spherical polar coordinate)
V_d	= driving voltage
v	= mean radial velocity (cylindrical polar coordinate)

v_θ	= mean polar velocity (spherical polar coordinate)
x	= axial coordinate (cylindrical coordinate)
$x_{o,b}$	= virtual origin based on width
$x_{o,u}$	= virtual origin based on velocity
Δ	= centerline peak-to-peak deflection of the membrane
ε	= eddy viscosity in the Schlichting solution
ϵ	= eddy viscosity in the Landau–Squire solution
η	= self-similar variable (Schlichting solution)
θ	= polar coordinate (spherical polar coordinate)
$\theta_{1/2}$	= half-angle of the jet
ξ	= self-similar variable (Landau–Squire solution)
ρ	= density of the fluid
τ	= total shear stress

I. Introduction

A SYNTHETIC jet or a zero-net-mass-flux (ZNMF) jet is a type of fully periodic jet that results from the formation and interaction of vortex rings or pairs [1]. A common method of generating a synthetic jet employs a cavity-diaphragm setup and is the method used in this investigation. The synthetic jet generator consists of a sealed cavity with a flexible vibrating diaphragm on one end and an orifice on the other. As shown in Fig. 1, the synthesis is composed of a cycle with two strokes: namely, a suction and an ejection. During the suction stroke, the diaphragm moves away from the orifice, increasing the volume of the cavity and subsequently decreasing the pressure within. This results in the entrainment of low-momentum fluid into the cavity. During the ejection stroke, the diaphragm moves toward the orifice, resulting in the expulsion of fluid through the orifice. At the edge of the orifice, the formed shear layer rolls up to form a vortex ring that travels downstream due to its self-induced velocity. In this fashion, a series of suction–ejection strokes results in the formation of a train of vortex rings moving away from the orifice. These coherent structures then interact, coalesce, and break down in a transition toward a turbulent jet that is directed downstream.

Received 28 December 2008; revision received 28 April 2009; accepted for publication 4 May 2009. Copyright © 2009 by the American Institute of Aeronautics and Astronautics, Inc. All rights reserved. Copies of this paper may be made for personal or internal use, on condition that the copier pay the \$10.00 per-copy fee to the Copyright Clearance Center, Inc., 222 Rosewood Drive, Danvers, MA 01923; include the code 0001-1452/09 and \$10.00 in correspondence with the CCC.

*Graduate Student, Department of Aerospace Engineering.

†Associate Professor, Department of Aerospace Engineering. Associate Member AIAA.

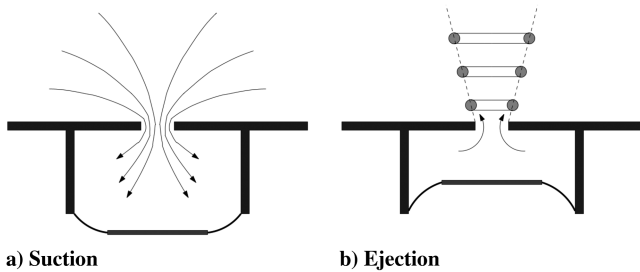


Fig. 1 Schematic of synthetic jet operation displaying the suction and ejection strokes.

This operational principle allows for the synthetic jet to be synthesized entirely from the surrounding medium, which consequently implies a zero net mass flux across the actuator boundary. However, on account of the asymmetry of the system, a net momentum flux is imparted to the external flow. The lack of plumbing provides an added benefit of reduced size, weight, and fabrication complexity. Additionally, the periodic vortex rings introduced into the flow exhibit an ability to influence the environment at a variety of length scales. All of these properties make synthetic jets attractive in a number of applications that include active flow control [2–4], electronic cooling [5,6], fluid mixing [7], and aerial [8–11] and underwater propulsion [12,13]. Although recent reviews of synthetic jets may be found in the literature [14–16], a brief overview of the background relevant to the present investigation is presented next.

Synthetic jet actuators occur primarily in axisymmetric [17–19], and rectangular [1,20,21] configurations, depending on the geometry of the external flowfield that is to be influenced. The axisymmetric type is studied in this paper, in which the flow structure of the issuing jet is dependent upon several characteristics that include the geometry of the actuator, fluid properties, and actuation parameters. Two nondimensional variables (namely, the stroke ratio L/d and Reynolds number Re) are identified as the primary factors that influence synthetic jets [1]. The stroke ratio is representative of the length of the slug of fluid ejected from the orifice during the expulsion stroke. The stroke ratio may also be interpreted as an inverse Strouhal number, where $2\pi/(L/d) = St$ [22], and the Reynolds number embodies the velocity of this ejected slug. The explicit definitions are given later in the paper. In addition, because the formation of a synthetic jet is incumbent upon the ejected vortex rings escaping the flow entrained back into the cavity during the suction stroke, a criterion for jet formation [23,24] in an axisymmetric case is given as

$$\frac{1}{2\pi} \frac{L}{d} > 0.16$$

The flowfield of an issuing synthetic jet may be thought to be composed of a near field and a far field based on the dominant flow phenomena, and a schematic of the evolution of the jet is presented in Fig. 2. The near field is typified by the presence of discrete coherent vortex rings and fully periodic flow. The flow in the far field is, by contrast, directed solely away from the orifice and bears resemblance to a turbulent continuous jet. This likeness is in the form of the self-similarity of the flow as inferred from the collapse of the scaled mean and turbulent intensity profiles [1,17]. The synthetic jets are observed, however, to spread faster and decay more rapidly than their continuous turbulent counterpart [17,18]. This points to the fact that synthetic jets possess an enhanced capacity for mixing. It is this self-similar behavior and increased spreading rate, which suggests that turbulent jet similarity models may be extended to synthetic jets by taking into account the enhanced mixing present in synthetic jets. Thus, in this paper, we hypothesize that round synthetic jets in the far field may be modeled using similarity analysis just as round continuous turbulent jets are modeled, with an adjustment of the virtual eddy viscosity coefficient of the continuous jet. Accordingly, the jet is systematically modeled to obtain the virtual viscosity associated with a synthetic jet from the spreading and decay rates,

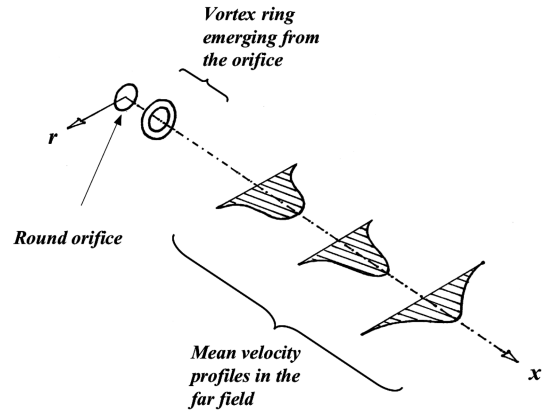


Fig. 2 Schematic of the evolution of a round synthetic jet, showing a vortex ring in the near field, and mean velocity profiles of the jet in the far field.

with experiments conducted to verify the aforementioned eddy viscosity replacement hypothesis. The effect of the key actuator parameters on the eddy viscosity is later examined.

This paper is outlined as follows: Section II describes the theoretical models for the external flowfield of the synthetic jet, followed by a model of the actuator. The experimental setup for the measurement of the velocity field and diaphragm deflection is then described in Sec. III. The results are presented and discussed in Sec. IV. In Sec. V, the conclusions are summarized.

II. Theoretical Modeling

In this section, models of the external flowfield of the round synthetic jet are first outlined, following which a model characterizing the synthetic jet actuator is presented.

A. Time-Averaged Flowfield

Consider the region of the synthetic jet in which the periodically formed vortex rings cease to be coherent discrete structures and a turbulent jet is directed downstream (Fig. 2). As mentioned earlier, the mean streamwise velocity profiles have been observed to collapse onto a single curve when scaled appropriately. It is this streamwise region that lends itself to similarity analysis. Two classic solutions to free continuous jets are the Schlichting [25] and the Landau–Squire [26,27] solutions. The first is based on boundary-layer approximations in cylindrical polar coordinates, and the second is a solution of the Navier–Stokes equations in spherical polar coordinates. Both solutions are outlined next with their applicability to synthetic jets discussed.

1. Schlichting Jet

The far field of a continuous jet may be thought to be generated by a continuous point source of momentum in an infinite incompressible fluid. It is admissible to describe the mean velocities in the continuous jet by boundary-layer equations. In seeking a self-similar solution to the boundary-layer equations, the streamwise pressure gradient is necessarily zero, whereupon a closed-form solution for a laminar jet exists [25]. It was later seen [28] that the turbulent jet analog could be modeled using the identical differential equations that described the laminar jet, with the sole replacement of the laminar viscosity coefficient with a virtual eddy viscosity coefficient associated with the turbulent jet. Following along these lines, it is hypothesized here that the mean velocity field of a synthetic jet may be modeled as a laminar free jet, along with the use of a virtual viscosity coefficient obtained empirically for a synthetic jet. An overview of the similarity analysis is traced out next, along with its pertinence to synthetic jets.

In polar coordinates, the boundary-layer equations with no pressure gradient are written as

$$\frac{\partial u}{\partial x} + \frac{\partial v}{\partial r} + \frac{v}{r} = 0, \quad u \frac{\partial u}{\partial x} + v \frac{\partial u}{\partial r} = \frac{1}{\rho r} \frac{\partial(r\tau)}{\partial r} \quad (1)$$

where u and v are the streamwise and radial velocity components, respectively; τ is the total shear stress; and ρ is the fluid density. The total shear stress may be related to the mean velocity using an eddy viscosity approximation:

$$\tau = \rho(v + \varepsilon_r) \frac{\partial u}{\partial r} = \rho \varepsilon \frac{\partial u}{\partial r} \quad (2)$$

where ν is the laminar kinematic viscosity, ε_r is the turbulent eddy viscosity coefficient, and ε is the total or effective eddy viscosity that takes into account both the laminar and turbulent contributions to the shear stress. Although the eddy viscosity hypothesis assumes that momentum transfer in a turbulent flow is dominated by large-scale eddies, it does characterize the mixing due to turbulent fluctuations, which in turn is indicative of the rate of spreading of a free jet.

The eddy viscosity may be derived from the experimental data as follows. Assuming that the evolution of the jet is dependent only on local length and velocity scales and lacks memory of the orifice dimensions itself, the streamwise mean velocity profiles may be considered self-similar. From the conservation of streamwise momentum, it may be shown that the characteristic length b and velocity u of the jet scale as x and x^{-1} , respectively. The self-similar assumption then leads to a streamwise velocity profile of the form $u = x^{-1}f(r/x)$. The similarity variable, written as $\eta = \sigma(r/x)$, is related to the virtual viscosity coefficient through a free constant σ . With the mixing length hypothesis showing that the virtual viscosity is constant over the entire jet, the boundary-layer equations may then be reduced to an ordinary differential equation of the form $ff' = f' - \eta f''$. From the conservation of momentum and the assumed form of the velocity distribution, the streamwise velocity is solved to be

$$u = \frac{3K}{8\pi\epsilon x} \frac{1}{(1 + \frac{1}{4}\eta^2)^2} \quad (3)$$

with the self-similarity variable given as

$$\eta = \frac{1}{4} \sqrt{\frac{3}{\pi}} \frac{\sqrt{K} y}{\epsilon r} \quad (4)$$

where K is the kinematic momentum of the jet, which is a measure of the strength of the jet, and is obtained as

$$K = 2\pi \int_0^\infty u^2 r dr$$

It is important to note here that the preceding analysis assumes a constant momentum flux in the streamwise direction. Although this is applicable to continuous jets, in synthetic jets, it has been reported that the momentum flux at the orifice is higher than that in the far field [1,21]. The momentum flux was shown to decrease in the near field of the jet due to an adverse pressure gradient and then to asymptote in the far field to some fraction of the exit momentum flux. It is this reduced asymptotic value of the momentum flux that should serve as the magnitude of the driving momentum flux in the preceding similarity analysis for the synthetic jet and not the exit momentum flux at the orifice of the actuator.

The eddy viscosity ε is now obtained from the spreading and decay rates of the jet. At the centerline, the streamwise velocity may be expressed as

$$u_c = \frac{3K}{8\pi\epsilon x} = S_u \frac{1}{x} \quad (5)$$

where S_u is a measure of the jet decay rate. The radial extent of the jet at a particular axial station may be characterized by a half-width $b_{1/2}$, defined as the radial distance from the centerline at which the streamwise velocity drops to half the centerline velocity. The linear streamwise variation of the half-width may be written as

$$b_{1/2} = S_b x \quad (6)$$

where S_b is the spreading rate of the jet. From Eqs. (3–6), the free constant σ in the similarity variable is related to the spreading rate as

$$\sigma = \frac{2\sqrt{\sqrt{2}-1}}{S_b} \quad (7)$$

from which the eddy viscosity is related to the spreading rate and decay rate as

$$\varepsilon = \frac{1}{8(\sqrt{2}-1)} \frac{S_b^2}{S_u} \quad (8)$$

In summary, Eqs. (3) and (8) model the far field of the jet in cylindrical coordinates. Thus, in this study, we employ the same technique (as previously discussed) in which the eddy viscosity of the synthetic jet is obtained from experimentally determined spreading and decay rates. Next, an alternative similarity model to a synthetic jet is presented.

2. Landau–Squire Jet

In this section, a solution of the Navier–Stokes equations to an axisymmetric free jet in spherical coordinates is outlined (Landau–Squire solution [26,27]). With the Schlichting solution, in seeking a self-similar solution to the boundary-layer equations, the streamwise pressure gradient was required to be zero. However, in the Landau–Squire jet, a self-similar solution to the Navier–Stokes equations exists for a laminar jet, without the requirement of a nonexistent pressure gradient. In replacing the viscosity coefficient of the laminar jet with the virtual viscosity of a turbulent jet, the velocity distribution of the turbulent jet model was found to be in good agreement with experiments [27]. As with the Schlichting model, the viscosity replacement hypothesis is extended to synthetic jets here, in which the salient results of the Landau–Squire solution are briefly presented.

The analysis in the slender viscous region comprising the jet and in the limiting behavior of high Reynolds number yield the radial velocity and pressure distributions as [29]

$$u_r = \frac{4\epsilon}{RC} \frac{1}{(1 + \xi^2)^2}, \quad p - p_\infty = \frac{4\epsilon^2}{R^2 C} \frac{\xi^2 - 1}{(1 + \xi^2)^2} \quad (9)$$

where ϵ is the virtual kinematic viscosity of the jet, the similarity variable is $\xi = \theta/\sqrt{2C}$, and C is a constant that is shown to be inversely proportional to a Reynolds number, which is based on the centerline velocity of the jet and distance from the origin. In the limit as $Re \rightarrow \infty$, C is expressed in terms of the magnitude of the point force that drives the jet, F , as

$$\frac{F}{2\pi\rho\epsilon^2} \rightarrow \frac{16}{3C} \quad (10)$$

The half-spreading angle $\theta_{1/2}$ is defined as the angle at which the radial velocity along a constant radius is half the centerline radial velocity $u_{r,c}$. Through the use of the definition of the half-spreading angle, the constant C is derived as

$$C = \frac{\theta_{1/2}^2}{2(\sqrt{2}-1)} \quad (11)$$

From which the virtual viscosity is shown to be

$$\varepsilon = \frac{1}{8(\sqrt{2}-1)} \frac{\theta_{1/2}^2}{S_u} \quad (12)$$

The virtual kinematic viscosity is thus a product of the inverse of the centerline velocity decay rate (which is identical in both cylindrical and spherical coordinates) and the square of the spreading angle of the jet and is of same form as that obtained from the Schlichting

solution. Thus, Eqs. (9–12) model the free jet in a spherical coordinate system. To enable this solution for a synthetic jet, the spreading angle and centerline decay rate need to be obtained from experiment.

Hitherto, models for the far field of continuous jets have been modified by the use of an adjusted eddy viscosity to apply to synthetic jets. With continuous steady jets, the critical nondimensional parameter of interest is a Reynolds number Re based on the steady exit bulk velocity. However, the upshot of the fully periodic nature of synthetic jets is as follows:

1) A steady bulk exit velocity does not exist, and hence a suitable average velocity needs to be defined.

2) Some way of characterizing the oscillatory nature of the flow is required.

These issues are addressed in the next section.

B. Actuator Model

As mentioned earlier, a nondimensional stroke ratio L/d and Reynolds number Re have been established as key actuator operational parameters that influence a synthetic jet [1]. For the cavity-diaphragm setup used in this experiment, they are obtained from an incompressible flow model, in which it is assumed that the volume displaced by the membrane is equal to the volume ejected from the orifice (Fig. 3). To obtain the volume displaced by the membrane, the shape of the deflected membrane and the central amplitude are required. The shape is obtained from the classical theory of plates [30], and the center amplitude is measured using a laser sensor. With the ejected volume approximated as a cylindrical slug of fluid with the same cross section as the exit orifice, the conservation of volume is written as

$$\alpha \frac{\pi D^2}{4} \Delta = \frac{\pi d^2}{4} L \quad (13)$$

where α is the fraction of the volume displaced by an imaginary piston undergoing a peak-to-peak deflection of Δ and is expressed as

$$\alpha = \frac{2\pi \int_0^{D/2} y(r)r dr}{(\pi D^2/4)\Delta} \quad (14)$$

where $y(r)$ is the deflection profile of the diaphragm. In assuming that the shape of the membrane is modeled by the static deflection of the circular membrane clamped on the edge subject to a uniform load, the deflection profile is written as

$$y(r) = \frac{\Delta}{2} \left[1 - \frac{r^2}{R^2} + \frac{2r^2}{R^2} \ln\left(\frac{r}{R}\right) \right] \quad (15)$$

where r is the radial coordinate and R is the radius of the membrane. The preceding deflection profile results in an α of 0.25. The nondimensional stroke ratio is then determined to be

$$\frac{L}{d} = \alpha \Delta \frac{D^2}{d^3} \quad (16)$$

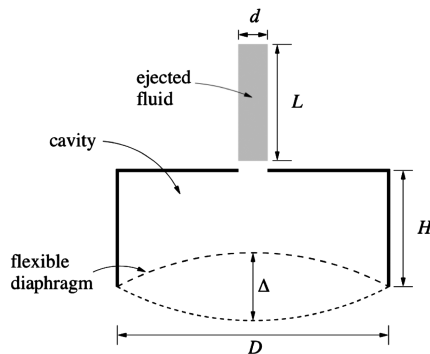


Fig. 3 Schematic of the actuator model, in which the volume of fluid displaced by the diaphragm is ejected through the orifice in the form of a slug.

The periodic nature of synthetic jets allows for the velocity scales to be defined based on either volume or momentum flux [31]. If based on volume flux, the velocity scale is given as $U_o = L/T = fL$, and if based on momentum flux, it is given as $U_o = \sqrt{2(L/T)} = \sqrt{2}fL$. It is more appropriate to use the velocity scale based on momentum flux here, as the self-similar jet solutions employed in this study define equivalent jets based on the same momentum flux and not mass flux. Consequently, the Reynolds number is defined as

$$Re = \frac{U_o d}{\nu} = \frac{\sqrt{2}fLd}{\nu} = \frac{\sqrt{2}f\alpha\Delta D^2}{\nu d} \quad (17)$$

The Reynolds number is explicitly seen to vary, with both membrane driving frequency and amplitude and with the stroke ratio appearing to be independent of frequency. This independence of stroke ratio on frequency is not accurate, as the use of a piezoelectric diaphragm as a driver gives rise to the coupling between frequency and deflection and, consequently, stroke ratio. However, for purposes of calculating the jet parameters, the model serves the purpose. In summary, Eqs. (16) and (17) express the dependency of the critical actuator parameters on the diaphragm driving frequency and deflection amplitude.

The preceding described flow and actuator models provide a framework to relate the input driving parameters (f, V_d) to the output jet parameters (S_u, S_b) via the actuator variables (L/d and Re). The experimental setup used to determine the empirical relationships between the various parameters is described next.

III. Experimental Method

From Sec. II, it is seen that the inputs to a synthetic jet model include 1) the central deflection of the membrane, 2) the spreading rate of the jet, and 3) the centerline velocity decay of the jet. In this section, the experimental setup to measure the aforementioned parameters are described.

A. External Flowfield

The experimental setup to characterize the flowfield is shown in Fig. 4. It consists of the synthetic jet actuator, computer-controlled stages, and a hot-wire probe, all of which were placed in a clear, large, Plexiglas enclosure (not shown). Piezoelectrically driven actuators were used in this experiment, and Fig. 5 is a picture of one such actuator. The actuator consists of a circular piezoelectric membrane sandwiched between two circular aluminum elements, which, when screwed together, form a cavity with an orifice on one end and a flexible membrane on the other. Three actuators were used in this study, the dimensions of which are stated in Table 1. The piezoelectric membrane is driven by a sinusoidal input voltage, the frequency and amplitude of which are varied and noted later.

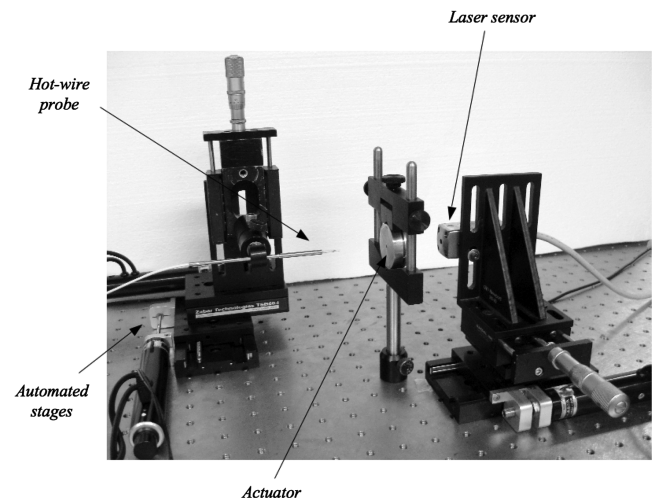


Fig. 4 Experimental setup used to measure the velocity field and diaphragm deflection.

attached to a movable automated stage and the diaphragm fixed in a particular location, the laser is moved in increments of $1 \mu\text{m}$ toward the diaphragm, with the signal response measured at each location. This nonlinear displacement-response curve then serves as the calibration curve. To make measurements, the laser is positioned at the location that allows for the largest sensitivity over the measurable range. To estimate the overall measurement accuracy of the laser, the uncertainties associated with stage position, sensor resolution, calibration, and experimental repeatability were taken into account. For a typical value, the total combined uncertainty was estimated by the root sum square to be $\pm 1 \mu\text{m}$.

The laser measurements were further validated using a noncontact inductance displacement sensor. The inductance sensor works on the principle that when a metal target (brass shim of the diaphragm) is introduced into the electromagnetic field emitted by the inductive sensor, a change in field strength is observed. This change is then registered as an output through the use of electronic circuitry, in which the proximity of the target to the sensor effects the output voltage. Through means of calibration, the output voltage is interpreted as a deflection.

IV. Results and Discussion

First, results of the dynamic response of the piezoelectric membrane are presented, following which the external flowfield is characterized.

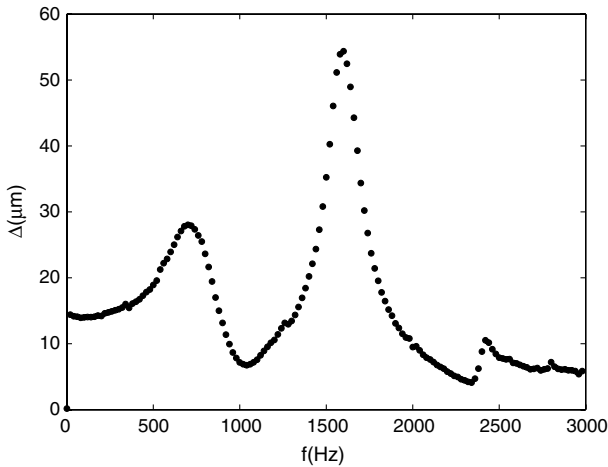


Fig. 8 The dependence of the dynamic deflection response (Δ) at the center of the piezoelectric membrane on driving frequency (actuator 1, $V_d = 10 \text{ V}$).

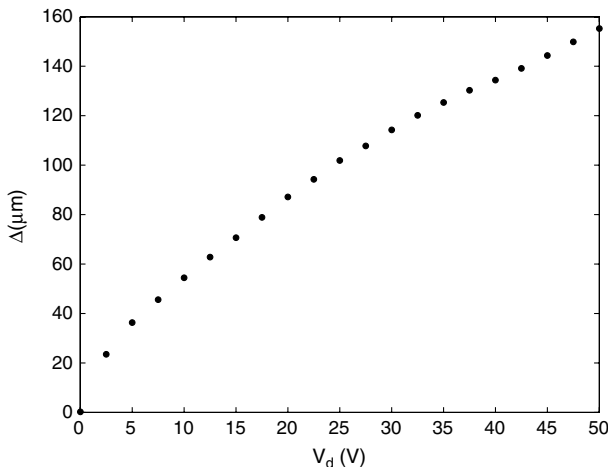


Fig. 9 The dependence of the dynamic deflection response at the center of the diaphragm on driving voltage (actuator 1, $f = 1600 \text{ Hz}$).

Table 2 Test Matrix for actuator 1, displaying the driving frequency f , voltage V_d , and corresponding nondimensional actuator parameters L/d and Re

Case no.	f	V_d	L/d	Re
1	1600	20	3.9	1324
2	1600	30	5.2	1765
3	1600	40	6.1	2070
4	1600	50	7.0	2376
5	1480	50	4.0	1256
6	1720	50	3.9	1460

A. Diaphragm Deflection

A synthetic jet with a cavity-diaphragm setup is a coupled system consisting of an electromechanical domain in the form of the diaphragm and a fluidic/acoustic domain in the form of the resonant cavity. The system may be thought to possess two fundamental frequencies: one associated with the resonant frequency of the diaphragm and the other with the Helmholtz frequency of the cavity.

To determine the fundamental frequencies of the system, the driving voltage was fixed and the frequency was swept in intervals of 20 Hz over the range of 0–3000 Hz, with the laser sensor measuring the central dynamic response of the membrane. Figure 8 shows the frequency response for actuator 1 operating at 10 V, where three peaks are seen. The first peak may be associated with the acoustic resonant frequency of the cavity. From analytical calculations of the fundamental frequency of a clamped circular plate [34], the second peak at 1600 Hz is associated with the diaphragm resonant frequency in mode (0,1) and is additionally observed to maximize the exit mean velocity downstream of the orifice.

Next, the effect of the driving voltage at a fixed frequency was studied. With the frequency fixed at 1600 Hz, the driving voltage was swept over the range of 0 to 50 V in intervals of 2.5 V. The dynamic response is seen to increase with an increase in driving voltage (Fig. 9). With the other actuators, similar trends in the frequency and amplitude response were observed as well.

The preceding deflection results permit the selection of the frequency that maximizes the membrane deflection and provides the centerline deflection of the membrane, which serves as an input to the actuator model described. As seen from the frequency response curve, the amplitude of vibration and frequency are tied in together and thus do not permit the study of the effect of frequency independently of amplitude over a wide range. With the preceding constraint in mind, experiments with varying driving parameters were conducted, and the test matrix for actuator 1 is summarized in Table 2. For cases 1 through 4, the driving frequency was fixed at 1600 Hz (the frequency that maximized the exit velocity) with the driving voltage varied, resulting in a variation in both stroke ratio and Reynolds number. Cases 5 and 6 were both run at a voltage of 50 V, at two different frequencies that resulted in the same stroke ratio but different Reynolds numbers. The latter two cases were conducted to evaluate the effect of Reynolds number on the external flow.

B. External Flowfield

1. Schlichting Model

Figure 10 shows the streamwise development of the centerline mean velocity u_c of the jet for test cases 1 through 4 for actuator 1. Two regions are clearly observed: the first region (referred to as the developing region) is where the velocity is seen to either increase (as in case 1) or remain constant. The second region (referred to as the developed region) exhibits a decay in velocity. Because of the limitations of the single hot-wire probe in highly oscillatory flow, measurements closer than that reported could be not be trusted. However, other workers [35] have reported an initial increase in velocity close to the orifice and have attributed this to the acceleration of the flow due to the presence of a standing vortex ring at the orifice [17,35].

Figure 11 shows the centerline decay, and the streamwise distance is scaled by the stroke length for each case. The extent of the

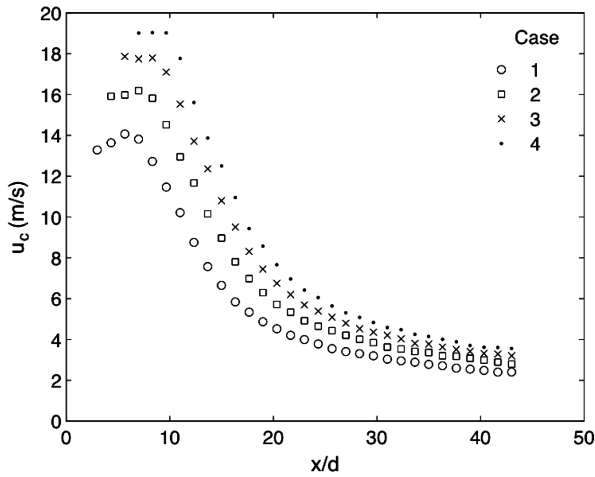


Fig. 10 The evolution of the mean centerline velocity u_c with streamwise distance x/d for different test cases (see Table 2 for details on cases).

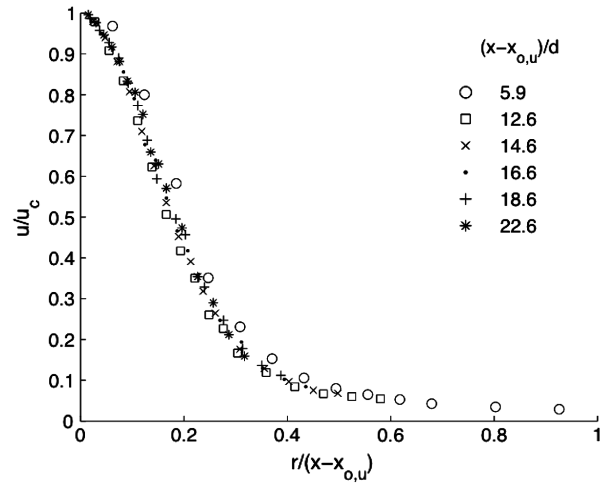


Fig. 12 Normalized streamwise velocity profiles u/u_c at different streamwise distances from the virtual origin $x_{o,u}$ in cylindrical coordinates.

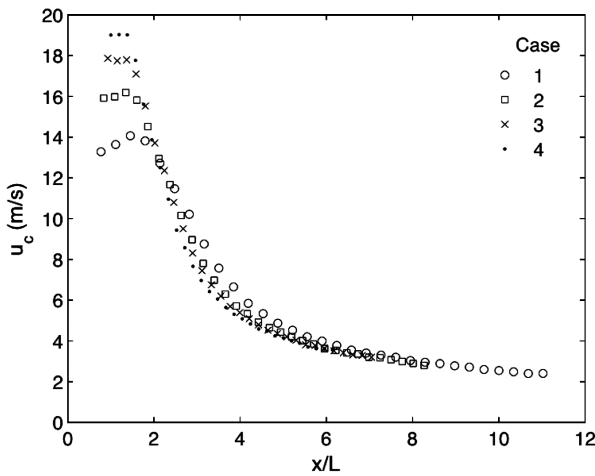


Fig. 11 Variation of centerline velocity with the scaled axial distance x/L , showing the extent of the developing region scaling with stroke length.

developing region is now clearly seen to scale with stroke length, and in about 1.5 stroke lengths, the mean velocity starts to decay, signaling the start of jetlike behavior. This can be reasoned as follows. The spacing between individual vortex rings is proportional to stroke length [36]; thus, an increase in stroke length makes for a longer distance over which the initial interaction of rings takes place. This scaling of the extent of the developing region was noticed in the other actuators as well; however, the size of this region varied from actuator to actuator.

In the developed region, to demonstrate the self-similarity as inferred from the mean flow, Fig. 12 presents the normalized mean velocity profiles at different axial locations downstream of the orifice for case 3. The velocity is scaled by the centerline velocity u_c , and the radial distance is scaled by the axial distance from the virtual origin of velocity $x_{o,u}$. Within a few diameters of the orifice, the jet begins to spread and slow down. The scaled velocity profiles appear to collapse rather well onto a Gaussian-like profile; however, it appears that the profile closest to the orifice $[(x - x_{o,u})/d = 5.9]$ exhibits some deviation, suggesting that the jet has not fully reorganized itself or developed at this streamwise location.

With the self-similar behavior established in the developed region, the variation of the centerline mean velocity with axial distance may be expressed as

$$\frac{U_o}{U_c} = K_u \left(\frac{x - x_{o,u}}{d} \right) \quad (19)$$

where K_u is a scaled measure of the decay rate of the jet, and $x_{o,u}$ is the axial location of the virtual origin of U_o/U_c . It was mentioned earlier that the actuator exit momentum flux is not equal to the momentum flux of the synthetic jet at the streamwise location at which self-similarity is achieved. However, we continue to use the exit momentum flux (or otherwise, U_o) to scale the jet, as the asymptotic value of the momentum flux is not readily available.

The dependence of K_u and $x_{o,u}$ on L/d is shown in Fig. 13, in which both the decay rate and location of the virtual origin increase with stroke ratio. The increasing trend in decay rate is observed in the other actuators as well; however, the rates of increase differ, possibly due to different geometries and subsequent initial conditions at the orifice (Fig. 14). In evaluating the effect of Reynolds number on the decay rate, it was observed that cases 5 and 6 (see Table 2), which have similar stroke ratios ($L/d \approx 4$) and different Reynolds numbers, resulted in the same decay rate as in case 1. Although the variation in Reynolds number is only about 14%, the results suggest that the centerline velocity decay is independent of Reynolds number, as other workers have reported over a wider range of Reynolds number [19,35].

The growth of the jet is characterized by the spreading rate that may be expressed as

$$\frac{b_{1/2}}{d} = K_b \left(\frac{x - x_{o,b}}{d} \right) \quad (20)$$

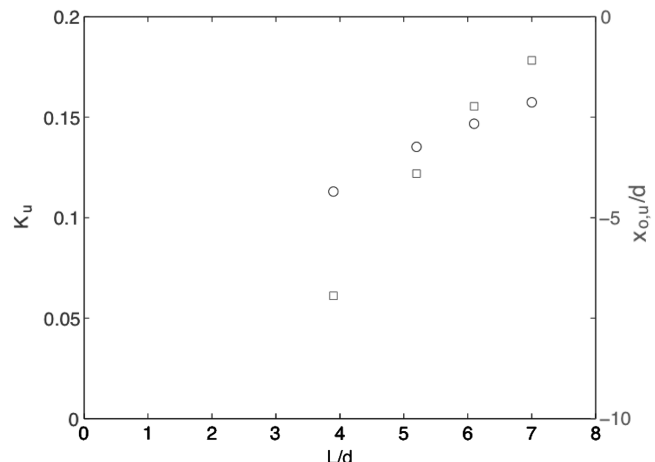


Fig. 13 Dependence of decay rate K_u (○) and location of the virtual origin $x_{o,u}$ (□) on stroke ratio.

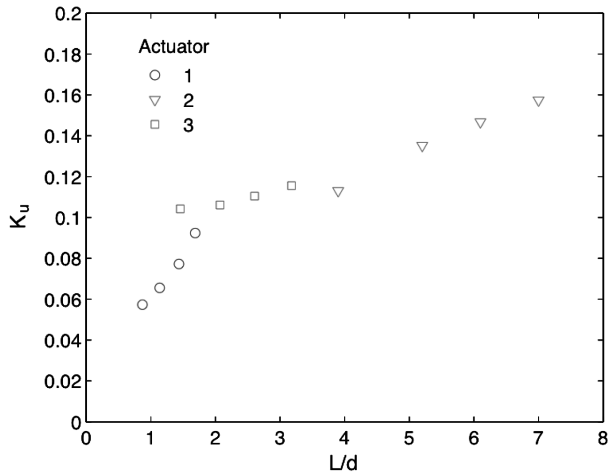


Fig. 14 Dependence of decay rate on stroke ratio, where K_u increases with L/d , however, at different rates depending on the actuator.

where $b_{1/2}$ is the half-width of the jet, K_b is the scaled spreading rate of the jet, and $x_{0,b}$ is the location of the virtual origin based on the jet width.

The variation in width of the jet (case 3) in the streamwise direction is shown in Fig. 15, in which a linear trend is seen. As seen in Fig. 16, the spreading rates increase with stroke ratio for all of the actuators, in

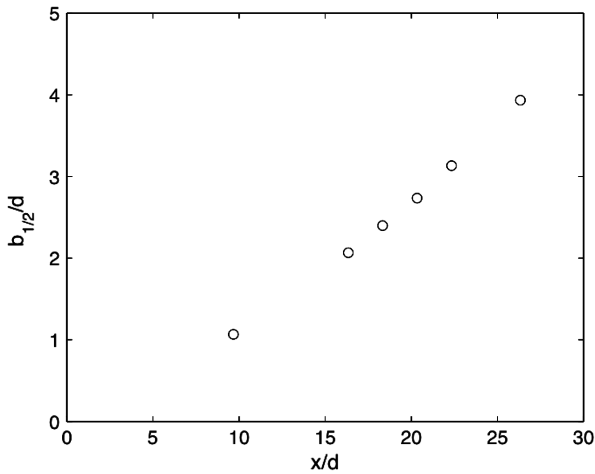


Fig. 15 Linear variation of jet width $b_{1/2}$ in the streamwise direction in cylindrical coordinates.

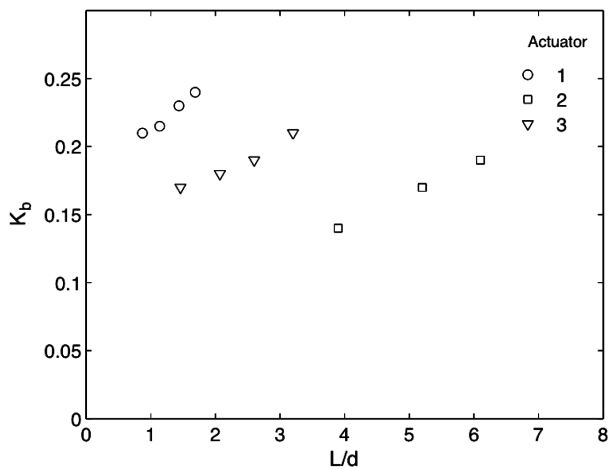


Fig. 16 Dependence of spreading rate K_b on stroke ratio, where K_b increases with L/d , however, at different rates depending on the actuator.

which the dependence on the actuator geometry is once again evident. In all cases seen here, the spreading rate of the synthetic jet exceeds that of continuous turbulent jets. Once again, cases 5 and 6 resulted in the same spreading rate as case 1, giving further credence to the lack of dependence of the aforementioned flow parameters on Reynolds number.

Figure 17 presents the variation of the calculated virtual viscosity [Eq. (8)] of the three actuators with stroke ratio. The eddy viscosity of the equivalent continuous jet is also shown for comparison. Synthetic and continuous jets of the same exit diameter d are considered to be equivalent in this investigation, based on momentum flux; otherwise, if the steady bulk exit velocity of a continuous jet is equal to the mean velocity of a synthetic jet, it is calculated as $U_o = \sqrt{2}fL$. The eddy viscosity of the synthetic jet is seen to far exceed that of continuous jets. The effect of employing a velocity scaling based on mass flux is to reduce the eddy viscosity, as reported in Fig. 17, by a factor of $\sqrt{2}$. With the eddy viscosity encompassing the capacity to transfer momentum to the surrounding fluid, it appears that the periodic nature of a synthetic jet greatly increases the momentum transfer in comparison with continuous jets. This higher eddy viscosity of the synthetic jet makes it appropriate for applications in which changes in the surrounding fluid are desired, as in fluid mixing or flow control. With the interaction of large-scale coherent vortical structures

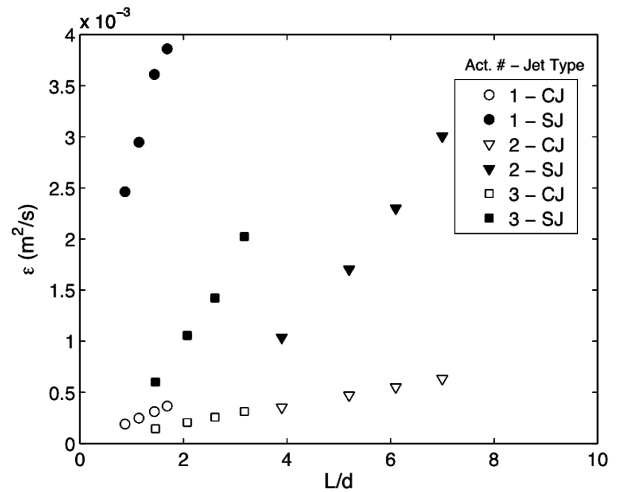


Fig. 17 Dependence of eddy viscosity ϵ on stroke ratio for three actuators, with the eddy viscosity of equivalent turbulent continuous jets shown for comparison.

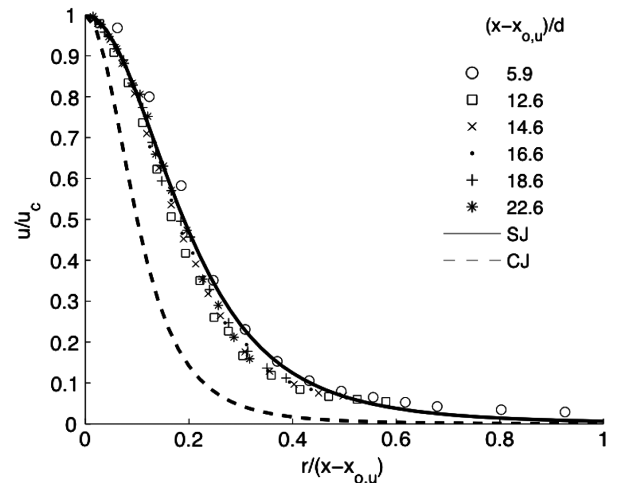


Fig. 18 Comparison of the analytical Schlichting model with experimental normalized velocity profiles. The solution for the synthetic jet is shown in a solid line, and for comparison purposes the solution for a continuous turbulent jet is shown in a dashed line.

primarily responsible for mixing and spreading in the near field, it may be argued that an increase in stroke length increases the volume, impulse, and energy associated with issuing vortex rings, thereby enhancing the interactions and mixing in the jet.

Equation (3), along with the empirically determined virtual viscosity, models the mean streamwise velocity profile, as shown in Fig. 18. The velocity profile of a continuous turbulent jet of equivalent momentum flux with a spreading rate of 0.1 is presented for comparison. Here, we explicitly see the enhanced mixing present in the synthetic jet in comparison with a continuous jet. The Schlichting model approximates the data well, validating the eddy viscosity replacement hypothesis.

To further reinforce the enhanced momentum transfer in synthetic jets, the axial development of turbulence intensity is presented in Fig. 19. In the developing region, extremely high turbulent intensities have been reported [35]. However, beyond the developing region, as seen from the plot, the turbulent intensity decreases in the streamwise direction and appears to asymptote to a turbulent intensity that increases with stroke length. This further suggests that the influence of the increased stroke ratio is felt not only in the mean velocity but also in the turbulent components. It is known that when the turbulence intensity is high (greater than 30%) or when flow reversal occurs, significant errors are introduced in using a single hot-wire [37]. From Fig. 19, the region in which the hot-wire results may be thought to be valid based on the preceding turbulence intensity

criteria varies with the L/d . Thus, as L/d increases, the axial distance beyond which the hot-wire results may be thought to be quantitatively valid increases as well. Thus, for $L/d = 3.9$, the distance at which $u'/u_c < 0.3$ is approximately $20d$, and for $L/d = 7$, it is $28d$. As mentioned earlier, measurements made before the preceding axial locations may be interpreted qualitatively or understood to be subject to errors associated with high turbulence intensity.

Figure 20 shows the streamwise turbulent intensity profiles in which the turbulent fluctuations and lateral distance are normalized by the centerline velocity and streamwise distance from the virtual origin, respectively. As may be inferred from Fig. 19, in the streamwise range shown in Fig. 20, the turbulent intensity profiles are still evolving and have not yet reached a self-similar state. This is quite like other shear flows, in which the higher-order moments become self-similar further downstream, in comparison with the mean velocity, as the turbulence reacts more slowly to local conditions [38].

2. Landau–Squire Model

As discussed, the Schlichting jet solution (which is a solution to the boundary-layer equations in cylindrical polar coordinates) models the velocity profiles of the synthetic jet in the far field, with the use of an empirically determined virtual viscosity. The Landau–Squire model, which is a solution to the Navier–Stokes equations in

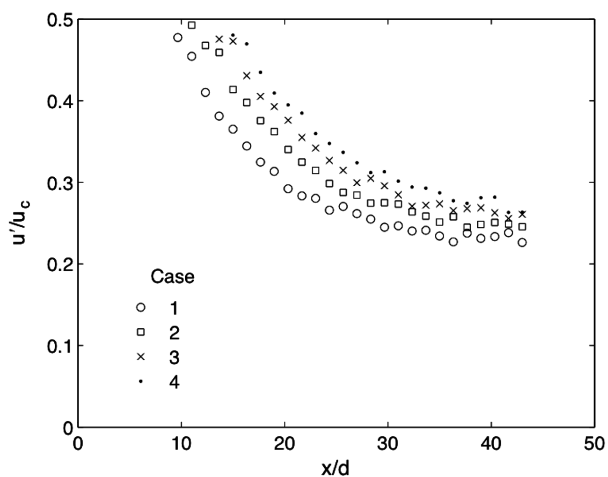


Fig. 19 Variation of the centerline streamwise turbulent intensity u'/u_c with axial distance for different test cases (see Table 2 for details on cases).

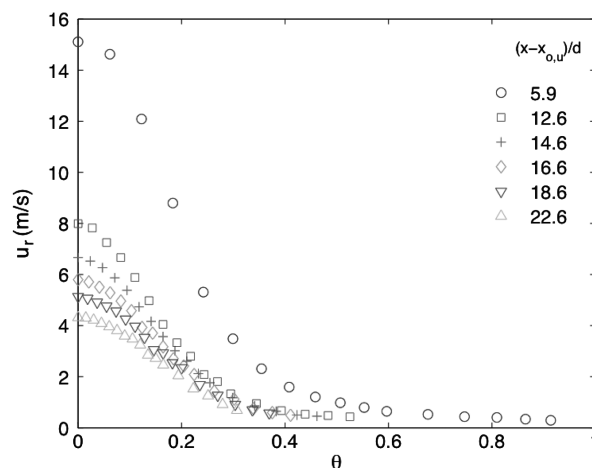


Fig. 21 Radial velocity profiles of a synthetic jet, in spherical polar coordinates, at different radial stations downstream of the orifice.

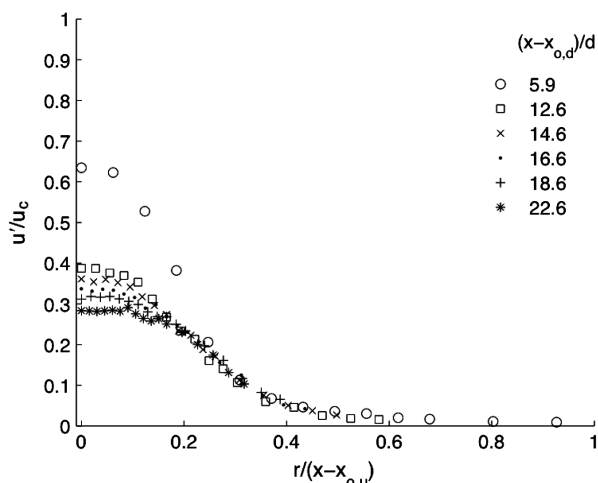


Fig. 20 Normalized streamwise turbulence intensity profiles at different streamwise distances from the virtual origin in cylindrical coordinates, in which the intensity profiles continue to develop.

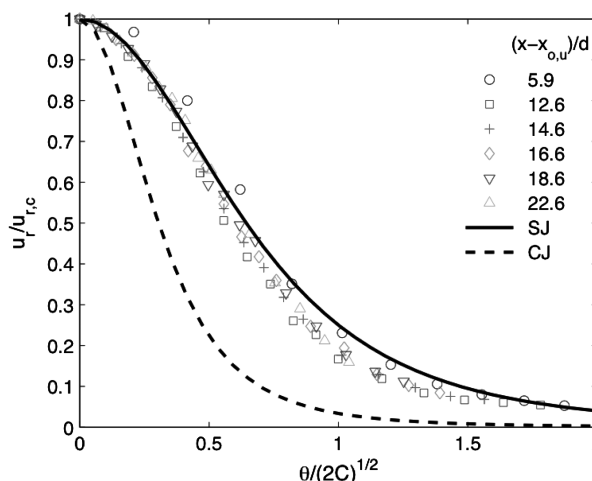


Fig. 22 Comparison of the analytical Landau–Squire model with the experimental normalized velocity profiles; solution for the synthetic jet (solid line) and, for comparison purposes, solution for a continuous turbulent jet (dashed line).

spherical polar coordinates, is seen to be equally agreeable to modeling the experimental data. Figure 21 shows the radial velocity profiles at different radial locations. With the profiles presented in spherical polar coordinates, the jet, as expected, is seen to slow down and spread. The centerline decay is identical to that shown in Fig. 10, as the radial (in spherical system) and axial (in cylindrical system) coordinates are coincident at the centerline, thus leading to the same decay rates K_u , as shown in Fig. 14. The variation in half-spreading angle with radial distance downstream of the orifice is seen to remain fairly constant.

If the radial velocity and polar angle are normalized as suggested by Eq. (9), the velocity profiles at different radial locations collapse onto a single curve (Fig. 22). By using the measured decay rate and spreading angle, the eddy viscosity is obtained through Eq. (12), following which the analytical velocity profile is obtained from Eq. (9). As seen in Fig. 22, the analytical solution agrees well with the experimental data, in which the turbulent continuous jet was seen to be narrower than an equivalent synthetic jet. Thus, it is possible to conclude that the Landau–Squire model is equally accommodating to modeling the far field of a synthetic jet.

V. Conclusions

The external flowfield of a round synthetic jet was studied using hot-wire anemometry. Two regions, as distinguished by the centerline velocity, were observed: an initial developing region in which coherent periodic vortex rings exist and start to interact and a developed region in which the vortical structures break down to turbulence and the jet exhibits characteristics of a round continuous turbulent jet. The extent of the developing region is seen to scale with the stroke length while changing from one actuator to another. In the developed region, the mean velocity profiles exhibit self-similar behavior, with the centerline velocity decaying as x^{-1} and jet width increasing as x , just as with a continuous turbulent jet. This similitude to continuous jets leads to the hypothesis that the synthetic jet may be modeled as a continuous turbulent jet using self-similar solutions, with the replacement of the eddy viscosity of a turbulent jet with that associated with a synthetic jet. The synthetic jet is modeled using both the Schlichting solution to boundary-layer equations in cylindrical polar coordinates and the Landau–Squire solution to the Navier–Stokes equations in polar coordinates. It is further shown that, similar to a continuous turbulent jet, the eddy viscosity of a synthetic jet can be obtained from the spreading and decay rates of the jet. The experiments on the flowfield validate this hypothesis, further showing that the eddy viscosity of the synthetic jet is larger than an equivalent turbulent jet. In this study, synthetic and turbulent jets are considered to be equivalent, based on the sameness of momentum flux. This enhanced eddy viscosity is attributed to the additional mixing brought about by the initial introduction of the periodic vortical structures and their ensuing breakdown and transition to turbulence. Therefore, by using the adjusted value of the virtual viscosity, the theoretical models of a continuous turbulent jet may still be used to model a periodic synthetic jet. The velocity decay rate and spreading rate of synthetic jets are observed to increase with stroke ratio while being independent of Reynolds number within the limited range investigated. The geometry of the actuator is, however, seen to have an impact on the decay and spreading rates by means of influencing the initial conditions at the orifice. This dependency of spreading and decay rate on stroke ratio is accredited to the increased impulse, energy, and subsequent enhanced interactions of individual vortex rings emerging from the orifice as the stroke ratio increases. In summary, the semi-analytical method proposed here for synthetic jets connects the external flowfield, as characterized by the spreading rate K_b and velocity decay rate K_u , to the actuator input driving functions V_d and f via the actuator parameters L/d and Re .

Acknowledgments

The authors thank Yury Vargas for his initial contribution to the experiment and Jean Hertzberg for her initial help with the hot-wire calibration.

References

- [1] Smith, B., and Glezer, A., "The Formation and Evolution of Synthetic Jets," *Physics of Fluids*, Vol. 10, No. 9, 1998, pp. 2281–2297. doi:10.1063/1.869828
- [2] Amitay, M., Smith, B., and Glezer, A., "Aerodynamic Flow Control Using Synthetic Jet Technology," 36th Aerospace Sciences Meeting and Exhibit, AIAA Paper 98-0208, Reno, NV, 1998.
- [3] Seifert, A., Eliahu, S., Greenblatt, D., and Wygnanski, I., "Use of Piezoelectric Actuators for Airfoil Separation Control," *AIAA Journal*, Vol. 36, No. 8, 1998, pp. 1535–1537. doi:10.2514/2.549
- [4] Rathnasingham, R., and Breuer, K., "Active Control of Turbulent Boundary Layers," *Journal of Fluid Mechanics*, Vol. 495, 2003, pp. 209–233. doi:10.1017/S0022112003006177
- [5] Mahalingam, R., and Glezer, A., "Design and Thermal Characteristics of a Synthetic Jet Ejector Heat Sink," *Journal of Electronic Packaging*, Vol. 127, No. 2, 2005, pp. 172–177. doi:10.1115/1.1869509
- [6] Pavlova, A., and Amitay, M., "Electronic Cooling Using Synthetic Jet Impingement," *Journal of Heat Transfer*, Vol. 128, No. 9, 2006, pp. 897–907. doi:10.1115/1.2241889
- [7] Davis, S. A., and Glezer, A., "Mixing Control of Fuel Jets Using Synthetic Jet Technology," 37th Aerospace Sciences Meeting and Exhibit, AIAA Paper 99-0447, Reno, NV, 1999.
- [8] Parviz, B., Najafi, K., Muller, M., Bernal, L., and Washabaugh, P., "Electrostatically Driven Synthetic Microjet Arrays as a Propulsion Method for Micro Flight. Part 1: Principles Of Operation, Modelling, and Simulation," *Microsystem Technologies*, Vol. 11, No. 11, 2005, pp. 1214–1222. doi:10.1007/s00542-005-0599-0
- [9] Finley, T., and Mohseni, K., "Micro Pulsatile Jets for Thrust Optimization," 2004 ASME International Mechanical Engineering Congress, Paper 2004-62042, Anaheim, CA, 2004.
- [10] Vargas, Y., and Mohseni, K., "Characterization and Thrust Optimization of Synthetic Jets," 2006 ASME Joint U.S.—European Fluids Engineering Summer Meeting, American Society of Engineers, Paper 2006-98312, Miami, FL, 2006.
- [11] Krishnan, G., and Mohseni, K., "On the Modeling of a Synthetic Jet as a Spherical Jet," 5th Joint ASME/JSME Fluids Engineering Conference, American Society of Engineers Paper 2007-37306, San Diego, CA, 2007.
- [12] Mohseni, K., "Pulsatile Vortex Generators for Low-Speed Maneuvering of Small Underwater Vehicles," *Ocean Engineering*, Vol. 33, No. 16, 2006, pp. 2209–2223. doi:10.1016/j.oceaneng.2005.10.022
- [13] Krieg, M., and Mohseni, K., "Thrust Characterization of a Bio-Inspired Vortex Ring Generator for Locomotion of Underwater Robots," *Journal of Oceanic Engineering*, Vol. 33, No. 2, 2008, pp. 123–132. doi:10.1109/JOE.2008.920171
- [14] Glezer, A., and Amitay, M., "Synthetic Jets," *Annual Review of Fluid Mechanics*, Vol. 34, 2002, pp. 503–529. doi:10.1146/annurev.fluid.34.090501.094913
- [15] Tang, H., Zhong, S., Jabbal, M., Garcillan, L., Guo, F., Wood, N., and Warsop, C., "Towards the Design of Synthetic-Jet Actuators for Full-Scale Flight Conditions. Part 2: Low-Dimensional Performance Prediction Models and Actuator Design Method," *Flow, Turbulence and Combustion*, Vol. 78, Nos. 3–4, 2007, pp. 309–329. doi:10.1007/s10494-006-9061-3
- [16] PanFeng, Z., JinJun, W., and LiHao, F., "Review of Zero-Net-Mass-Flux Jet and Its Application in Separation Flow Control," *Science in China, Series E (Technological Sciences)*, Vol. 51, No. 9, 2008, pp. 1315–1344. doi:10.1007/s11431-008-0174-x
- [17] Mallinson, S., Hong, G., and Reizes, J., "Some Characteristics of Synthetic Jets," 30th AIAA Fluid Dynamics Conference, AIAA Paper 1999-3651, Norfolk, VA, 1999.
- [18] Cater, J., and Soria, J., "The Evolution of Round Zero-Net-Mass-Flux Jets," *Journal of Fluid Mechanics*, Vol. 472, 2002, pp. 167–200.
- [19] Shuster, J., and Smith, D., "Experimental Study of the Formation and Scaling of a Round Synthetic Jet," *Physics of Fluids*, Vol. 19, No. 4, 2007, pp. 45109–1–21.
- [20] Smith, B., and Swift, G., "A Comparison Between Synthetic Jets and Continuous Jets," *Experiments in Fluids*, Vol. 34, No. 4, 2003, pp. 467–72.
- [21] Fugal, S. R., Smith, B. L., and Spall, R. E., "Displacement Amplitude Scaling of a Two-Dimensional Synthetic Jet," *Physics of Fluids*,

- Vol. 17, No. 4, 2005, pp. 045103–1–10.
- [22] Holman, R., Utturkar, Y., Mittal, R., Smith, B., and Cattafesta, L., “Formation criterion for synthetic jets,” *AIAA Journal*, Vol. 43, No. 10, 2005, pp. 2110–2116.
doi:10.2514/1.12033
- [23] Utturkar, Y., Holman, R., Mittal, R., Carroll, R., Sheplak, B., and Cattafesta, L., “A Jet Formation Criterion for Synthetic Jet Actuators,” 41st Aerospace Sciences Meeting and Exhibit, AIAA Paper 2003-0636, Reno, NV, 2003.
- [24] Gallas, Q., Holman, R., Nishida, T., Carroll, B., Sheplak, M., and Cattafesta, L., “Lumped Element Modeling of Piezoelectric-Driven Synthetic Jet Actuators,” *AIAA Journal*, Vol. 41, No. 2, 2003, pp. 240–247.
doi:10.2514/2.1936
- [25] Schlichting, H., “Laminare Strahlausbreitung,” *ZAMM*, Vol. 13, No. 4, 1933, pp. 260–263.
doi:10.1002/zamm.19330130403
- [26] Landau, L., “A New Exact Solution of the Navier–Stokes Equations,” *Doklady Akademii Nauk SSSR*, Vol. 43, 1944, pp. 286–288.
- [27] Squire, H., “The Round Laminar Jet,” *Quarterly Journal of Mechanics and Applied Mathematics*, Vol. 4, No. 3, 1951, pp. 321–329.
- [28] Schlichting, H., *Boundary Layer Theory*, 2nd ed., McGraw–Hill, New York 1955
- [29] Sherman, F., *Viscous Flow*, McGraw–Hill, New York 1990.
- [30] Timoshenko, S., *Theory of Plates and Shells*, McGraw–Hill, New York 1999.
- [31] Smith, B., and Swift, G., “Synthetic Jets at Larger Reynolds Number and comparison with Continuous Jets,” 31st AIAA Fluid Dynamics Conference and Exhibit, AIAA Paper 2001-3030, Anaheim, CA, 2001.
- [32] Johnstone, A., Uddin, M., and Pollard, A., “Calibration of Hot-Wire Probes Using Nonuniform Mean Velocity Profiles,” *Experiments in Fluids*, Vol. 39, No. 3, 2005, pp. 525–532.
- [33] Tavoularis, S., *Measurement in Fluid Mechanics*, Cambridge Univ. Press, New York, 2005.
- [34] Blevins, R. D., *Formulas for Natural Frequency and Mode Shape*, Krieger, Malabar, FL, 1995.
- [35] Di Cicca, G. M., and Iuso, G., “On the Near Field of an Axisymmetric Synthetic Jet,” *Fluid Dynamics Research*, Vol. 39, Nos. 9–10, 2007, pp. 673–693.
doi:10.1016/j.fluidyn.2007.03.002
- [36] Mohseni, K., and Gharib, M., “A Model for Universal Time Scale of Vortex Ring Formation,” *Physics of Fluids*, Vol. 10, No. 10, 1998, pp. 2436–2438.
doi:10.1063/1.869785
- [37] Hussein, H., Capp, S., and George, W., “Velocity-Measurements in a High-Reynolds-Number, Momentum-Conserving, Axisymmetrical, Turbulent Jet,” *Journal of Fluid Mechanics*, Vol. 258, 1994, pp. 31–75.
doi:10.1017/S002211209400323X
- [38] Pope, S., *Turbulent Flows*, Cambridge Univ. Press, New York, 2000.

A. Plotkin
Associate Editor